Limitations of reactive atomistic potentials in describing defect structures in oxides

2016 Modelling Simul. Mater. Sci. Eng. 24 035022

(http://iopscience.iop.org/0965-0393/24/3/035022)

IOP Publishing Modelling and Simulation in Materials Science and Engineering

Modelling Simul. Mater. Sci. Eng. **24** (2016) 035022 (17pp) doi:10.1088/0965-0393/24/3/035022

Limitations of reactive atomistic potentials in describing defect structures in oxides

Teemu Hynninen[1], Tiziana Musso[2] and Adam S Foster[2,3]

[1] Wihuri Physical Laboratory, Department of Physics and Astronomy, University of Turku, FI-20014 Turku, Finland
[2] COMP, Department of Applied Physics, Aalto School of Science, PO Box 11100, FI-00076 Aalto, Finland
[3] Division of Electrical Engineering and Computer Science, Kanazawa University, Kanazawa 920- 1192, Japan

E-mail: teemu.hynninen@utu.fi

Received 9 October 2015, revised 20 January 2016
Accepted for publication 5 February 2016
Published 16 March 2016

Abstract

It is difficult to achieve low expense and high accuracy in computational methods, yet it remains a key objective in atomistic approaches. In solid state physics, advanced atomistic potentials using reactive force fields have shown promise in delivering both. However, these methods have not been applied widely beyond their development environment and thus their strengths and weaknesses are not fully understood. In this work we present benchmark calculations on silica (SiO_2) and hafnia (HfO_2) structures, comparing a leading charge optimized many-body potential to a more advanced density functional calculation. We find that although the atomistic potential gives excellent results for bulk structures, it has severe shortcomings when applied to small systems with low coordinated atoms. We also establish clearly the components of the many-body potential and how these relate to predicted physical properties.

Keywords: oxides, many-body potentials, computational methods, defects

(Some figures may appear in colour only in the online journal)

1. Introduction

In all fields of computational physics, including more complexity and accuracy in computational models improves the accuracy and reliability of the obtained results but comes at the cost of increased computational cost. Especially quantum mechanical calculations are usually computationally very demanding and therefore phenomenological and semi-classical models are interesting as cheap alternatives. In solid state physics, density functional theory (DFT) [1]

is often the method of choice being one of the most efficient quantum mechanical methods, which can handle systems of even thousands of atoms. Still, even DFT is usually too expensive if one wishes to analyse very large systems or sample a set of systems in order to obtain statistics. More efficient, but less precise methods include for example tight binding models [2] and empirical potentials [3–5].

By empirical potentials we refer to methods where electrons are not explicitly included in the model (often described as force field models or even just atomistic potentials). Instead, the electronic contribution to the behaviour of the system is taken into account by describing the interactions between atoms using an effective potential energy which is a function of only the positions of the atomic nuclei. This approach obviously cannot give information on properties that require explicit knowledge of the properties of the electrons, such as charge transfer and bond creation/breaking. However, if one is interested in structural properties, calculations can be made more efficient by several orders of magnitude if electrons need not be included in the model. Advanced atomistic potentials include more degrees of freedom than just the positions of atoms [6], but are still much more efficient than quantum mechanical techniques. For instance the ReaxFF [7] and charge-optimized many body (COMB) [8] families of potentials also take into account atomic charges, i.e. partial electron transfer, in order to improve the description of electrostatic interactions, and these potentials have shown promising results in the description of organic molecules [7, 9] and solid state materials such as silicon and silica [8, 10] as well as several metal oxides [6, 11–13].

In general, atomistic potentials are constructed by choosing a way to represent the potential energy function as well as a relevant set of reference data such as experimental results or results from more advanced levels of theory. The representation may be built from mathematical functions, chosen using physical insight [14–17]. Alternatively, the representation can be constructed without assuming any particular functional form using tabulation or automated procedures such as machine learning [18, 19]. These potentials are typically characterized by a large number of parameters which are fitted to the reference data. This is a difficult problem, but if done well, the resulting potential can describe the system at least in some part of the phase space. The fitting procedure makes sure the potential reproduces the properties that were included in the reference data, but it depends on the mathematical representation whether interpolation and extrapolation is successful beyond the points included in the reference data. Especially if a potential has been fitted against bulk properties, it may fail to describe clusters, and vice versa.

In this work, we test the COMB potential for describing defects in silica and hafnia. Silicon and its oxide are the key materials of the semiconductor industry, while hafnia is increasingly important as high dielectric insulators in modern devices [20]. However, as the scale of these devices is approaching the atomic scale, individual defects are having an ever increasing impact on device reliability [21–23]. Tools are needed for analysing and identifying the defects present in these materials and understanding how to control them. Computational analysis of individual defects can be done routinely with DFT [24], but more efficient yet sufficiently reliable methods are needed in order to dynamically simulate the formation of defects and sample the phase space for stable defect structures [25]. The family of COMB potentials has been parameterized for both of these materials and thus they potentially offer a set of tools for accomplishing this task.

COMB potentials have been constructed primarily to reproduce bulk and interface properties, and their reliability for describing defects and other irregular structures is less clear. We benchmark the potential against DFT by analysing a group of small silica clusters, whose properties are fairly well understood [26–28]. In addition, we study the demanding challenge of the diffusion of oxygen interstitials in hafnia, already extensively studied [29–31], allowing a direct comparison.

2. Methods

2.1. COMB potentials

The charge optimized many-body potentials (COMB) were introduced to allow large scale simulations of semiconductor and oxide materials [8]. Three versions of COMB exist with somewhat different formulation [6], representing different materials. In this work, we focus on the second generation of the COMB parameterization of silicon, silica, and hafnia [10, 11]. We refer to this formulation simply as COMB in the following.

COMB describes the atomic system in terms of atomic positions $\{\mathbf{r}\}$ and effective atomic charges $\{q\}$ which are both allowed to evolve dynamically. In a dynamic simulation, charges are assumed to respond to changes in the system much faster than atomic positions, and so charges are allowed to find an equilibrium after each change in the spatial coordinates. This can in principle be done using any non-linear optimization method. In the standard implementation of COMB, equations of motions are written also for the charges and a damping term is included to converge the trajectories to an equilibrium position. Note that energy is not conserved in this scheme, and so energy conserving dynamics cannot be simulated with this method alone. In this study, however, we only probe minimum energy configurations and do not consider dynamics at all. Next, we consider the components of COMB in detail, as there are some contradictions between existing literature and the approximations in the actual code being routinely used.

A fictious inertia M_q is assigned to the atomic charges and the system is described by the Lagrangian [32]

$$L(\{\dot{q}\},\{\dot{\mathbf{r}}\},\{q\},\{\mathbf{r}\}) = \sum_i \frac{1}{2} m_i \dot{\mathbf{r}}_i^2 + \sum_i \frac{1}{2} M_q \dot{q}_i^2 - U(\{q\},\{\mathbf{r}\}) - \nu \sum_i q_i, \quad (1)$$

where the last term is a Lagrange multiplier for the constraint of fixed total charge $Q = \sum_i q_i$. This leads to the equations of motion for the position and charge of atom α

$$m_\alpha \ddot{\mathbf{r}}_\alpha = -\nabla_\alpha U \quad (2)$$

$$M_q \ddot{q}_\alpha = -\frac{\partial U}{\partial q_\alpha} - \nu. \quad (3)$$

The term $\chi_\alpha = -\partial U/\partial q_\alpha$ is the inverse electronegativity, i.e. electropositivity of atom α. A direct calculation shows that $M_q \ddot{Q} = -\sum_i \partial U/\partial q_i - N\nu$, where N is the number of atoms, and so for fixed total charge we must have $\ddot{Q} = 0$ and $\nu = -1/N \sum_i \partial U/\partial q_i = \bar{\chi}$ is the average electropositivity [32]. Finally, in order to dissipate the kinetic energy associated with the dynamic charges, a dissipative term is added to (3). Thus, the equations of motion for the charges become

$$M_q \ddot{q}_\alpha = \chi_\alpha - \bar{\chi} - \eta_q \dot{q}_\alpha, \quad (4)$$

where η_q is an effective friction coefficient for the dynamic charges.

The COMB potential energy is given by

$$U = \sum_i U_i^{\text{self}} + \sum_{(i,j)} U_{ij}^{\text{mb}} + \sum_{(i,j,k)} U_{ijk}^{\text{bend}}, \quad (5)$$

where U_i^{self} is the self-energy of atom i, U_{ij}^{mb} contains pair and manybody interaction involving the bond between atoms i and j, and U_{ijk}^{bend} is the bond bending energy of the bonds between

atoms *i*-*j* and *j*-*k*. The summations go over all atoms i, all pairs (i, j) and all triplets (i, j, k), respectively. The mathematical formulation of these terms is described below, and values of all the numeric parameters are given in table 1.

The self energy of an atom describes the energy associated with charging an atomic site. In COMB, this is expressed as a polynomial and penalty terms (called 'barrier functions' in COMB)

$$U_i^{\text{self}} = \sum_{n=1}^{4} c_{i,n} q_i^n + c_{\min}\chi_{q_i<q_{\min}}(q_{\min} - q_i)^4 + c_{\max}\chi_{q_i>q_{\max}}(q_i - q_{\max})^4. \tag{6}$$

Here c are parameters and $\chi_{q<Q}$ is the characteristic function, which is 1 for $q < Q$ and 0 otherwise. This means an extra penalty term $c_{\min}(q_{\min} - q_i)^4$ is applied if the charge q_i is less than $q_{\min}$ and the term $c_{\max}(q_i - q_{\max})^4$ is added if q is greater than $q_{\max}$. This is meant to keep the charge q_i between the limits $q_{\min}$ and $q_{\max}$.

The bending term U_{ijk}^{bend} describes the energies associated with bending atomic bonds. For silica, the bond bending terms are applied for Si–O–Si and O–Si–O bond angles, while Hf–Hf–Hf angles are treated in hafnia. Altogether the contribution is

$$U_{ijk}^{\text{bend}} = U_{ijk}^{\text{Si-O-Si}} + U_{ijk}^{\text{O-Si-O}} + U_{ijk}^{\text{Hf-Hf-Hf}} \tag{7}$$

where

$$U_{ijk}^{\text{Si-O-Si}} = \chi_{ijk}^{(\text{Si,O,Si})} f_{ij}^R f_{jk}^R K_{ijk}^{(\text{Si,O,Si})}(\cos\theta_{ijk} - \cos\theta_{\text{Si-O-Si}})^2 \tag{8}$$

$$U_{ijk}^{\text{O-Si-O}} = \chi_{ijk}^{(\text{O,Si,O})} f_{ij}^R f_{jk}^R K_{ijk}^{(\text{O,Si,O})}(\cos\theta_{ijk} - \cos\theta_{\text{O-Si-O}})^2 \tag{9}$$

$$U_{ijk}^{\text{Hf-Hf-Hf}} = \chi_{ijk}^{(\text{Hf,Hf,Hf})} f_{ij}^R f_{jk}^R K_{ijk}^{(\text{Hf,Hf,Hf})} L_6(\cos\theta_{ijk}). \tag{10}$$

Here $\chi_{ijk}^{(\text{A,B,C})}$ is 1 only if the atoms (i, j, k) are a triplet $A - B - C$ of the corresponding elements and 0 otherwise, and L_6 is the sixth order Legendre polynomial. The functions f are cutoff functions for ensuring finite lengths for the bonds. These functions are defined as

$$f(r, r_{\text{soft}}, r_{\text{hard}}) = \begin{cases} 1, & r \leqslant r_{\text{soft}} \\ \dfrac{1}{2}\left[1 + \cos\left(\pi \dfrac{r - r_{\text{soft}}}{r_{\text{hard}} - r_{\text{soft}}}\right)\right], & r_{\text{soft}} < r \leqslant r_{\text{hard}} \\ 0, & r > r_{\text{hard}} \end{cases} \tag{11}$$

and they make the interactions disappear continuously as the atomic distance r changes from the soft cutoff r_{soft} to the hard cutoff r_{hard}. We use the shorthand notation $f_{ij}^R = f(r_{ij}, R_{\text{soft},ij}, R_{\text{hard},ij})$, where r_{ij} is the distance between atoms i and j and the cutoff radii, $R_{\text{soft},ij}$ and $R_{\text{hard},ij}$, are parameters.

The term U_{ij}^{mb} contains pair and manybody interactions,

$$U_{ij}^{\text{mb}} = U_{ij}^{\text{repulsive}} + U_{ij}^{\text{attractive}} + U_{ij}^{\text{Coulomb}} + U_{ij}^{\text{correction}}, \tag{12}$$

where the terms represent repulsive and attractive bonding potentials, the electrostatic potential, and additional corrections, respectively.

Given the maximum and minimum charges of an atom, $q_{\max}$ and $q_{\min}$, respectively, and the changes in atomic diameters associated with these charges, $d_{\max}$ and $d_{\min}$, as well as a scaling exponent n, the following derived parameters are calculated

Table 1. Values for the parameters used in the COMB potential.

Interaction	Parameter	Value	Reference
U_i^{self}	c_1	Si: 0, O: 5.634 41, Hf: 0	[10, 11]
U_i^{self}	c_2	Si: 3.625 14, O: 7.689 60, Hf: 3.139 52	[10, 11]
U_i^{self}	c_3	Si: 0, O: 4.514 27, Hf: 0	[10, 11]
U_i^{self}	c_4	Si: 0.087 07, O: 1.330 08, Hf: 0.009 41	[10, 11]
U_i^{self}	c_{min}	1000.0	Lammps
U_i^{self}	c_{max}	1000.0	Lammps
U_i^{self}	q_{min}	Si: −3.6, O: −1.651 41, Hf: −3.6	Lammps
U_i^{self}	q_{max}	Si: 3.6, O: 4.954 14, Hf: 3.6	Lammps
U_{ijk}^{bend}	K	Si–O–Si: 2.60, O–Si–O: 0.3122, Hf–Hf–Hf: 0.008	[10, 11]
several	R_{soft}	Si–Si: 2.8, O–O: 2.6, Hf–Hf: 3.65, Si–O: 2.55, Si–Hf: 3.11, Hf–O: 3.225	Lammps
several	R_{hard}	Si–Si: 3.0, O–O: 3.0, Hf–Hf: 4.05, Si–O: 3.05, Si–Hf: 3.41, Hf–O: 3.375	Lammps
U_{ij}^{mb}	q_{min}	Si: −4.0, O: −1.8349, Hf: −4.0	[10, 11]
U_{ij}^{mb}	q_{max}	Si: 4.0, O: 5.5046, Hf: 4.0	[10, 11]
U_{ij}^{mb}	d_{min}	Si: 1.651 725, O: 0.001 48, Hf: 0.261 52	[10, 11]
U_{ij}^{mb}	d_{max}	Si: −1.658 949, O: −0.001 12, Hf: −0.259 18	[10, 11]
U_{ij}^{mb}	n	10	[10, 11]
$U_{ij}^{\text{repulsive}}$	$\tilde{A}$	Si: 1830.80, O: 3326.699, Hf: 707.5303	Lammps
$U_{ij}^{\text{repulsive}}$	λ	Si: 2.4799, O: 5.36, Hf: 2.069 563	[10, 11]
$U_{ij}^{\text{attractive}}$	$\tilde{B}$	Si: 471.18, O: 260.893, Hf: 55.942 16	[10, 11]
$U_{ij}^{\text{attractive}}$	α	Si: 1.7322, O: 2.68, Hf: 0.959 614	[10, 11]
$U_{ij}^{\text{attractive}}$	β	Si: $1.1 \cdot 10^{-6}$, O: 2.0, Hf: 0.046 511	[10, 11]
$U_{ij}^{\text{attractive}}$	μ	Si: 3, O: 1, Hf: 1	[10, 11]
$U_{ij}^{\text{attractive}}$	η	Si: 0.787 34, O: 1, Hf: 1.011 011	[10, 11]
$U_{ij}^{\text{attractive}}$	c	Si: 100 390, O: 6.6, Hf: 0	[10, 11]
$U_{ij}^{\text{attractive}}$	d	Si: 16.218, O: 1, Hf: 1	[10, 11]
$U_{ij}^{\text{attractive}}$	h	Si: −0.598 26, O: −0.229, Hf: 0	[10, 11]
$U_{ij}^{\text{attractive}}$	b_{soft}	same as A_{soft}, except (Si–O)–O: 2.95, (Hf–Hf)–O: 3.225	Lammps
$U_{ij}^{\text{attractive}}$	b_{hard}	same as A_{hard}, except (Si–O)–O: 3.45 (Hf–Hf)–O: 3.375	Lammps
U_{ij}^{Coulomb}	ζ	Si: 0.772 871, O: 2.243 072, Hf: 0.679 131	[10, 11]
U_{ij}^{Coulomb}	σ	3.535 53	Lammps
U_{ij}^{Coulomb}	C_{soft}	11.5	—
U_{ij}^{Coulomb}	C_{hard}	12.0	Lammps
U_{ij}^{field}	ν_1	Si: −0.499 378, O: −3.922 011, Hf: −3.928 750	[10, 11]
U_{ij}^{field}	ν_2	Si: 2.999 911, O: 0.971 086, Hf: 4.839 580	[10, 11]
$U_{ij}^{\text{HfO-overcoordination}}$	E_{over}	0.16	[10]

(*continued*)

Table 1. (*Continued*)

Interaction	Parameter	Value	Reference
$U_{ij}^{\mathrm{HfO-overcoordination}}$	τ	0.10	[10]
$U_{ij}^{\mathrm{HfO-repulsion}}$	Ω	0.14	[10]
$U_{ij}^{\mathrm{HfO-repulsion}}$	r_1	2.2285	[10]
$U_{ij}^{\mathrm{HfO-repulsion}}$	r_2	1.8935	[10]
$U_{ij}^{\mathrm{HfO-repulsion}}$	R_{soft}	2.5135	Lammps
$U_{ij}^{\mathrm{HfO-repulsion}}$	R_{hard}	2.5635	Lammps
$U_{ij}^{\mathrm{HfO-repulsion}}$	$\tilde{R}_{\mathrm{soft}}$	1.9435	Lammps
$U_{ij}^{\mathrm{HfO-repulsion}}$	$\tilde{R}_{\mathrm{hard}}$	1.8935	Lammps

Note: All units are in terms of eV, Å and electron charges. The reference 'Lammps' refers to the COMB parameters provided with the potential included in Lammps simulation package and the hard coded values found in Lammps source code. In cases where the values reported in literature differ from those given in Lammps, the latter have been used.

$$\bar{q}_i = \frac{1}{2}(q_{\mathrm{min},i} + q_{\mathrm{max},i}) \tag{13}$$

$$\delta q_i = \frac{1}{2}(q_{\mathrm{max},i} - q_{\mathrm{min},i}) \tag{14}$$

$$a_i = \left(1 - \left|\frac{\bar{q}_i}{\delta q_i}\right|^{n_i}\right)^{-1} \tag{15}$$

$$m_i = \frac{\ln[d_{\mathrm{max},i}/(d_{\mathrm{max},i} - d_{\mathrm{min},i})]}{\ln[q_{\mathrm{max},i}/(q_{\mathrm{max},i} - q_{\mathrm{min},i})]} \tag{16}$$

$$g_i = \frac{(d_{\mathrm{min},i} - d_{\mathrm{max},i})^{1/m_i}}{q_{\mathrm{max},i} - q_{\mathrm{min},i}} \tag{17}$$

$$\tilde{g}_i = \frac{|a_i|^{1/n_i}}{\delta q_i}. \tag{18}$$

Also a charging function is defined as

$$D_i(q_i) = d_{\mathrm{max},i} + |g_i(q_{\mathrm{max},i} - q_i)|^{m_i}. \tag{19}$$

Here, equation (15) is defined according to [12, 33] which differ from the original formulation in [8].

Using these definitions and the additional parameters $\tilde{A}_i$ and λ_i, the repulsive potential is written

$$U_{ij}^{\mathrm{repulsive}}(r_{ij}, q_i, q_j) = f_{ij}^R A_{ij}(q_i, q_j)\mathrm{e}^{-\lambda_{ij} r_{ij}} \tag{20}$$

$$\lambda_{ij} = \frac{1}{2}(\lambda_i + \lambda_j) \tag{21}$$

$$A_{ij}(q_i, q_j) = \sqrt{A_i(q_i)A_j(q_j)} \tag{22}$$

$$A_i(q_i) = \tilde{A}_i \mathrm{e}^{\lambda_i D_i(q_i)} \tag{23}$$

The attractive part is similar,

$$U_{ij}^{\text{attractive}}(r_{ij}, q_i, q_j) = f_{ij}^R b_{ij} B_{ij}(q_i, q_j) \mathrm{e}^{-\alpha_{ij} r_{ij}} \tag{24}$$

$$\alpha_{ij} = \frac{1}{2}(\alpha_i + \alpha_j) \tag{25}$$

$$B_{ij}(q_i, q_j) = \sqrt{B_i(q_i)B_j(q_j)} \tag{26}$$

$$B_i(q_i) = \tilde{B}_i \mathrm{e}^{\alpha_i D_i(q_i)} [a_i - |\tilde{g}_i(\tilde{Q}_i - q_i)|^{m_i}], \tag{27}$$

but it also includes an extra charge scaling function in (27) and a Tersoff-type bond order factor b_{ij} [16] resulting in many-body interactions

$$b_{ij} = \frac{1}{2}(\tilde{b}_{ij} + \tilde{b}_{ji}) \tag{28}$$

$$\tilde{b}_{ij} = \left[1 + \left(\beta_j \sum_{k \neq i,j} \xi_{ijk}(r_{ij}, r_{jk}) \gamma_{ijk}(\theta_{ijk})\right)^{\eta_j}\right]^{-\frac{1}{2\eta_j}} \tag{29}$$

$$\xi_{ijk}(r_{ij}, r_{jk}) = f_{ij}^b \mathrm{e}^{\alpha_{ij}^{\mu_j}(r_{ij} - r_{jk})^{\mu_j}} \tag{30}$$

$$\gamma_{ijk}(\theta_{ijk}) = 1 + \frac{c_j^2}{d_j^2} - \frac{c_j^2}{d_j^2 + (h_j - \cos\theta_{ijk})^2}, \tag{31}$$

where β_j, μ_j, η_j, c_j, d_j, and h_j are parameters.

COMB includes the electrostatic interaction between charged atoms as a screened Coulomb interaction calculated between *s*-type Slater orbitals. In practice this means that atomic charges are represented by charge densities

$$\rho_i(\mathbf{r}) = q_i \frac{\zeta_i^3}{\pi} \mathrm{e}^{-2\zeta_i |\mathbf{r} - \mathbf{r}_i|}, \tag{32}$$

where $\mathbf{r}_i$ is the position of the atomic centre and ζ_i is a decay constant. Then, the Coulomb energy between atoms i and j is

$$E_{ij}^{\text{Coulomb}} = \frac{1}{4\pi\varepsilon_0} \int \frac{\rho_i(\mathbf{r})\rho_j(\mathbf{r}')}{|\mathbf{r} - \mathbf{r}'|} \mathrm{d}^3 r \mathrm{d}^3 r'. \tag{33}$$

This can be calculated analytically [34]. For two atoms of the same species, $\zeta_i = \zeta_j = \zeta$, the result is

$$E_{ij}^{\text{Coulomb}} = \frac{1}{4\pi\varepsilon_0} \frac{q_i q_j}{r_{ij}} \left[1 - \left(1 + \frac{11}{8}\zeta r_{ij} + \frac{3}{4}(\zeta r_{ij})^2 + \frac{1}{6}(\zeta r_{ij})^3\right) \mathrm{e}^{-2\zeta r_{ij}}\right], \tag{34}$$

and for different species, $\zeta_i \neq \zeta_j$, using the shorthand $\kappa_{ij} = \frac{\zeta_i^2 + \zeta_j^2}{\zeta_i^2 - \zeta_j^2}$, we obtain

$$E_{ij}^{\text{Coulomb}} = \frac{1}{4\pi\varepsilon_0}\frac{q_i q_j}{r_{ij}}\left[1 - (1-\kappa_{ij})^2\left(\frac{1}{4}(2+\kappa_{ij}) + \frac{1}{4}\zeta_i r_{ij}\right)\mathrm{e}^{-2\zeta_i r_{ij}}\right.$$
$$\left. - (1+\kappa_{ij})^2\left(\frac{1}{4}(2-\kappa_{ij}) + \frac{1}{4}\zeta_j r_{ij}\right)\mathrm{e}^{-2\zeta_j r_{ij}}\right]. \tag{35}$$

In general, we can separate the long range $1/r_{ij}$ and the exponentially decaying parts and write

$$E_{ij}^{\text{Coulomb}} = \frac{1}{4\pi\varepsilon_0}\frac{q_i q_j}{r_{ij}}[1 - u(\zeta_i, \zeta_j, r_{ij})], \tag{36}$$

where the exponential contribution u, due to the decay in Slater charge density (32), is defined through equations (34) and (35).

However, COMB is parameterized for a screened Coulomb interaction [35], where equation (36) is modified to

$$U_{ij}^{\text{Coulomb}} = \frac{1}{4\pi\varepsilon_0}\frac{q_i q_j}{r_{ij}}\left[\operatorname{erfc}\left(\frac{r_{ij}}{\sigma\sqrt{2}}\right) - u(\zeta_i, \zeta_j, r_{ij})\right] - \frac{1}{4\pi\varepsilon_0}\frac{1}{\sigma\sqrt{2\pi}}\sum_i^N q_i^2. \tag{37}$$

Technically, this corresponds to an Ewald summation without including the reciprocal space summation of long range interactions in a periodic system. The physical interpretation of the parameter σ is that it is the width of the gaussian charge densities screening the atomic charges.

Using screening ignores the long ranged part of the Coulomb interaction, but it also makes the sum (37) converge rapidly. In the Lammps version of COMB, the Coulomb sum is truncated using the transformation

$$\tilde{U}(r) = \begin{cases} U(r) - U(C_{\text{hard}}) - (r - C_{\text{hard}})U'(C_{\text{hard}}) & r < C_{\text{hard}} \\ 0 & r > C_{\text{hard}} \end{cases}, \tag{38}$$

where C_{hard} is a cutoff distance. This form ensures smooth termination of the potential energy and forces, i.e. $\lim_{r\to C_{\text{hard}}} \tilde{U}(r) = 0$ and $\lim_{r\to C_{\text{hard}}} \tilde{U}'(r) = 0$. In our own implementation of COMB (see Methods below), we have also compared this to truncation by a cutoff function

$$\tilde{U}(r) = f^C U(r). \tag{39}$$

and a discontinuous cutoff ($U(r)$ jumps to 0 at the cutoff). With long enough cutoffs, the difference between the methods is very small, although in dynamic simulations the differences will eventually accumulate to produce different trajectories. A discontinuous cutoff may also cause a drift in total energy, but in COMB this is usually minor compared to the energy lost during charge optimization.

Finally, COMB introduces a group of corrections to bias certain configurations and force the correct energetic order for the most common silica and hafnia polymorphs. These are the field, over-coordination, and repulsion correction.

$$U_{ij}^{\text{correction}} = U_{ij}^{\text{field}} + U_{ij}^{\text{HfO}-\text{overcoordination}} + U_{ij}^{\text{HfO}-\text{repulsion}}. \tag{40}$$

The field correction is applied to all atoms, over-coordination correction to Hf–O bonds, and the repulsion correction modifies the repulsive interaction between Hf and O.

The field correction is defined as

$$U_{ij}^{\text{field}} = \frac{1}{4\pi\varepsilon_0}\frac{1}{r_{ij}^5}(\nu_{i,1}q_i + \nu_{i,2}q_i^2 + \nu_{j,1}q_j + \nu_{j,2}q_j^2). \tag{41}$$

This follows the definition found in Shan *et al* [10] (where it is called the penalty function) and Lammps source code, not the one given by Devine *et al* [12]. The field correction is truncated using similar cutoff transformations (38) and (39) as the Coulomb potential. Since U^{field} is not exponentially decaying, the truncation effect is more pronounced here than for the screened Coulomb interaction. Still, the difference between different truncation methods is small for static configurations.

The Hf–O overcoordination correction is

$$U_{ij}^{\text{HfO-overcoordination}} = \chi_{ij}^{(\text{Hf,O})} f_{ij}^R E_{\text{over}} \left[\chi_{\Delta_i>0.2}\Delta_i\left(\frac{1}{1+\mathrm{e}^{\tau\Delta_i}}\right) + \chi_{\Delta_j>0.2}\Delta_j\left(\frac{1}{1+\mathrm{e}^{\tau\Delta_j}}\right)\right] \tag{42}$$

$$\Delta_i = \sum_k \chi_{ik}^{(\text{Hf,O})} f_{ik}^R - 7. \tag{43}$$

The summation in (43) goes over all the neighbors of atom i, essentially counting the number of neighbors. The function $\chi_{ik}^{(\text{Hf,O})}$ is 1 only if the atoms i and k are a Hf–O pair, ensuring only Hf–O bonds are considered. If the coordination of the atom is over 7 (Hf coordination in the monoclinic phase), $\Delta_i > 0$, and the correction penalizes such overcoordinated structures by increasing the energy. E_{over} and τ are parameters. Note that the coordination Δ_i is calculated for each atom but the overcoordination penalty is evaluated for each Hf–O bond.

Finally, the Hf–O repulsion correction is given by

$$U_{ij}^{\text{HfO-repulsion}} = U_{ij}^{\text{repulsive}} \chi_{ij}^{(\text{Hf,O})} f_{ij}^R \tilde{f}_{ij}^{\tilde{R}}\, \Omega\left(\frac{25}{4}x^4 - \frac{15}{4}x^2 + \frac{9}{16}\right) \tag{44}$$

$$x = \frac{r_1 - r_{ij}}{r_1 - r_2}, \tag{45}$$

where Ω, r_1 and r_2 are parameters and r_{ij} is the distance between atoms i and j. The function $\tilde{f}$ is a lower cutoff function similar to (11), except that $\tilde{r}_{\text{hard}} < \tilde{r}_{\text{soft}}$. That is, the function is 0 for $r < \tilde{r}_{\text{hard}}$ and 1 for $r > \tilde{r}_{\text{soft}}$. Note that the original repulsive potential $U_{ij}^{\text{repulsive}}$ is included in the term, i.e. the correction is multiplicative

$$U_{ij}^{\text{repulsive}} + U_{ij}^{\text{HfO-repulsion}} = (1 + \delta^{\text{correction}})U_{ij}^{\text{repulsive}}. \tag{46}$$

This behaviour is not clear from the definition in [11], but follows the implementation in Lammps.

2.2. Computational details

As a benchmark, all structures have been calculated using plane-wave density functional theory (DFT), as implemented in the VASP package [36]. The PAW [37, 38] method has been used along with the Perdew–Burke–Ernzerhof (PBE) [39] functional. All clusters simulations have been carried out in a $(20 \times 20 \times 20)$ Å cubic cell, with a kinetic energy cut-off of 500 eV and a Γ **k**-point. For the bulk structures, a $(3 \times 3 \times 3)$ Monkhorst-Pack mesh has been used. Convergence has been checked against cut-off energy and mesh sampling, within an accuracy

of 0.1 eV. The Bader algorithm [40, 41] was used for estimating the partial charges associated with each atom from the calculated charge densities. All structures were relaxed with a 0.01 eV Å^{-1} force convergence tolerance. In simulations of O diffusion in hafnia, a $(2 \times 2 \times 2)$ supercell of monoclinic hafnia with 96 atoms was used.

COMB calculations always used the relaxed VASP geometries and partial charges as the initial configuration and a new optimization of structures and charges was performed. The structural relaxation force tolerance was, as in DFT, 0.01 eV Å^{-1}. The convergence criterion used for charge equilibration was such that the maximum deviation from the average electronegativity had to be below a tolerance limit, $\max_i|\chi_i - \bar{\chi}| < 0.01$ V.

In our calculations, we use both the implementation in the Lammps package [42], written by the original developers of the potential, and our own implementation in the code Pysic [43] based on published literature and the source code of the Lammps version. Several bugs were found in the original Lammps implementation of the second generation COMB potential during this work. (These were reported to the developers and issues regarding silica potentials were fixed in the Dec 5 2013 patch for Lammps.) Due to these Lammps issues, we have used our own modified Lammps version in all calculations. We did not change the parameters file though, keeping on using the original COMB parameters [10, 11]. As a test of the robustness of the energy hierarchy predicted by COMB, we have tested reducing the Si–O attraction strength parameter by 10% from $B_{\mathrm{Si}--\mathrm{O}} = \sqrt{\bar{B}_{\mathrm{Si}}\bar{B}_{\mathrm{O}}} = 351$ to $B_{\mathrm{Si}-\mathrm{O}} = 320$. This parameterization is called 'COMB modified' in the text.

3. Results

3.1. Clusters

COMB has been parameterized against the energy hierarchy of various silica and hafnia bulk phases, reproducing them well [10, 11]. As a first test, we compare DFT and COMB results for bulk silica and hafnia. Fairly minor changes in bond lengths (0.02 Å) and angles (4°) are seen between the different methods for α-quartz silica and hardly any for the cubic silica phases. Similarly, for hafnia bulk phases, differences are notable only in the monoclinic phase, where bond lengths differ by less than 0.1 Å, and angles by less than 4°.

However, in order to accurately describe defects, where the local atomic bonding configuration differs from the bulk phase substantially, the potential also needs to replicate structures with low coordinated atoms. To test this, we compare a set of small clusters calculated with DFT and COMB. Relaxed Si_3O_n structures, calculated with DFT, COMB and COMB modified, are shown in figure 1.

Analysis of the configurational space reveals several local energy minima in the COMB potential of some of the clusters. For the smallest cluster shown in figure 1, Si_3O, COMB finds a metastable symmetric configuration, where the O atom has a local charge of $-1.5e$ and the neighboring Si have a charge of $0.9e$. However, COMB also finds a lowest-energy asymmetric configuration, where the neighboring silicon atoms have charges of $1.2e$ and $0.6e$. Due to Coulombic attraction, the Si with the higher charge is pulled closer to the O than the one with the lower charge. According to COMB, the energy of this configuration is in fact -0.1 eV lower than that of the symmetric configuration, making it the ground state configuration as predicted by COMB. A similar asymmetric COMB ground state is found for the Si_3O_2 cluster, where the energy difference between the lowest energy symmetric and asymmetric structures is about 0.2 eV. With larger clusters, the lowest energy is always found in the symmetric configuration. All the asymmetric states are unstable in DFT.

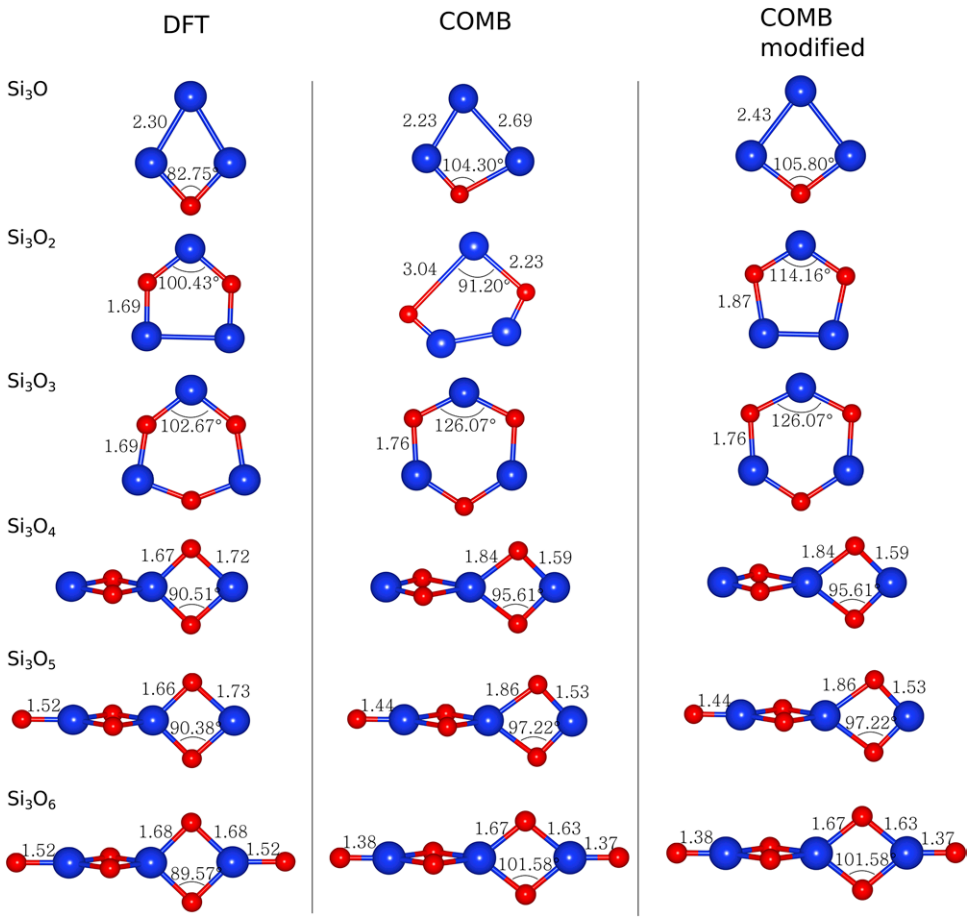

Figure 1. Comparison between Si_3O_n ($n = 1 \ldots 6$) clusters relaxed with DFT (left), COMB (center) and the modified COMB version (right). All lengths are in Å. Silicon atoms are blue, while oxygen ones are red.

As the metastable states of the smallest clusters are very close in energy, small modifications in COMB parameters will change the energy hierarchy of the different configurations. One simple way to make the symmetric configurations favorable in energy is changing the Si–O attraction strength ('COMB modified'). This potential finds a symmetric ground state for each cluster, although there are still quantitative differences to DFT structures. For instance, the Si–O–Si angles in the Si_3O and Si_3O_4 clusters are wider in COMB modified than in DFT by up to 20°. The same is true for O–Si–O angles in the Si_3O_2 and Si_3O_3 clusters and thus this is not an issue of COMB modified just overestimating the bond angle width of one type. Instead it appears that the bond angles depend on the local bonding environment in a more complicated way than what is reproduced in COMB. Similarly Si–O bond lengths vary, with COMB modified predicting longer and sometimes shorter bonds—the difference can be as large as almost 0.2 Å (Si_3O_2). For instance in the Si_3O_4 cluster, the relative lengths of the bonds is reversed in the COMB modified structure compared to DFT.

Similar comparison between DFT and COMB calculated hafnia clusters is shown in figure 2 and again considerable qualitative discrepancies between DFT and COMB are found

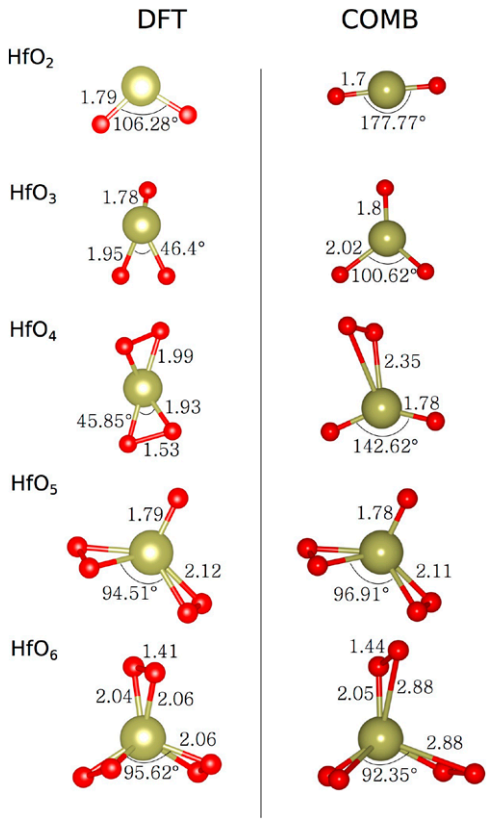

Figure 2. Comparison between relaxed structures obtained with DFT (left) and COMB (right) of HfO_n ($n = 2 \ldots 4$) clusters. All lengths are in Å. Hafnium atoms are yellow, while oxygen ones are red.

for the small clusters. COMB especially predicts wider bond angles than DFT, where the difference can be by a factor of 2. Bond lengths vary, so that in some cases DFT gives longer bonds while in others COMB does. Similarly to silica, larger clusters show a better agreement. Both calculation methods predict asymmetric clusters, which is not surprising considering the complicated structures hafnia forms also in bulk.

3.2. Oxygen diffusion in hafnia

As a test case of a real defect in a bulk material, we study the diffusion of oxygen in hafnia. This process has direct technological relevance and it has been extensively studied, making it an ideal benchmark system. Even though COMB fails to reproduce the DFT structures of small clusters, a point defect in bulk material is perhaps a lesser departure from the perfect bulk which the potential describes well, and better results could be expected.

We have chosen to simulate diffusion in the monoclinic phase of hafnia because it is the most stable phase at low temperatures [44], in fact it is commonly used as a gate-dielectric film in metal-oxide-semiconductor (MOS) transistors. Oxygen can diffuse through hafnia either with an exchange or interstitial mechanism, where generally the former is favored [45, 46]. Therefore we analyse structures where an additional O atom is placed at two different

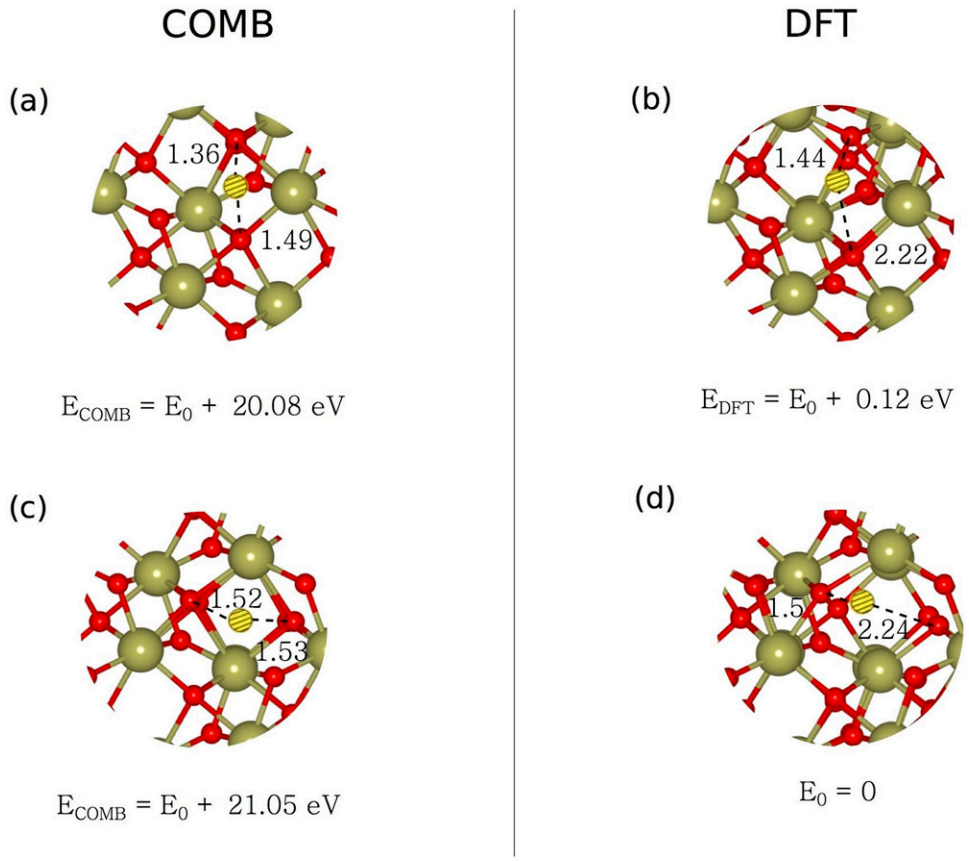

Figure 3. Interstitial oxygen as predicted by COMB and DFT at the beginning ((a), (b)) and the end ((c), (d)) of the diffusion process. Energies are referenced to the lowest energy configuration E_0. The defect oxygen atom is shown in dashed yellow. All lengths are in Å.

interstitial sites, corresponding to the initial and final configurations of the expected rate-limiting exchange process, as shown in figure 3.

In both cases, when starting from a configuration where the interstitial O atom is placed close to the centre of the interstitial volume, DFT predicts substantial relaxation of the structure, where several atoms are shifted by more than 0.5 Å. COMB relaxation also leads to some atoms shifting by 0.2/0.3 Å, but the interstitial O remains at the symmetric site, unlike the DFT calculation.

Even if the interstitial O atom is initially neutral [29], in the COMB-relaxed initial configuration it has a charge of $-0.34\ e$, while in the final one the charge becomes $-0.3\ e$, indicating that the interstitial O gets negatively charged as expected. To investigate the possibility of several local minima, the DFT-relaxed structures were recalculated with COMB. In both the initial and final configuration, COMB predicts metastable states similar to the DFT-structures (displacements are in the order of 0.05 Å), but these configurations are 1.2 eV and 2.1 eV higher in energy (according to COMB) than the more symmetric configurations obtained by starting the relaxation with the O atom at the centre of the interstitial volume. In other words, the problem of multiple local energy minima seen with the small clusters is seen also with the

interstitial defect, with the difference that this time DFT predicts an asymmetric ground state and COMB a symmetric one.

3.3. Bulk deformation

COMB fails for small clusters and point defects because it was originally optimised to reproduce bulk structures. Low coordinated atoms in clusters and point defects are not present in bulk lattices and therefore they are not represented in the data used in the construction of COMB. Extended defects and deformations are also important but less drastic deviations from the bulk, and so one should expect COMB to perform better when applied to such systems. Therefore as the final test, we examine deformed lattices using COMB and DFT.

We examine the α-quartz and β-cristobalite phases of silica and cubic hafnia under compression and shear. In the compression test, we allow the lattices to compress in one lattice direction by up to 20%, and in the shear test we allow one of the lattice directions to bend by up to 8°, corresponding to a lateral shift of 14% of the length of a lattice vector in the case of a cubic cell.

In all cases, DFT and COMB predict nearly identical structures for both materials when deformed. The sheared structures are shown in figure 4. As the structures are very similar to bulk, they are within the scope of COMB's applicability and these tests demonstrate that COMB is more reliable in describing lattice deformations than point defects.

However, COMB also produces a metastable structure with the same stoichiometry and supercell as the cristobalite structure, as shown in figure 4(d). The energy difference between the correct cristobalite lattice (b) and the metastable state (d) is 0.40 eV per atom. Although COMB predicts the correct ground state, the problem of unphysical local potential energy minima is present also here.

4. Discussion

DFT in general predicts a distinct ground state atomic structure, as the quantum mechanical potential energy is a fairly smooth function of the atomic coordinates. The COMB potential, on the other hand, includes spurious energy minima, i.e. non-physical metastable states close to the actual minimum energy configuration. This is a common problem of phenomenological potentials constructed from pair and many-body interactions [47] and it is not surprising to find this behavior also in COMB. Nonetheless, it means that simple optimization of structures carried out with the COMB potential will not necessarily find a physically valid structure. The problem appears to be the most severe with small clusters and defects, where local atomic coordination is very different from that found in bulk structures.

The energy hierarchy of the metastable states as predicted by COMB may be wrong, and the potential may give a qualitatively erroneous prediction of the ground state configuration. As seen in the presented test cases of clusters and defects, in some cases COMB predicts an asymmetric structure while DFT yields a symmetric one, and vice versa. This makes it very difficult to evaluate which configuration obtained with COMB, if any, corresponds to the real ground state, as the structures calculated from COMB all seem plausible. Furthermore, small changes in COMB parameters can change the hierarchy of the metastable states. If COMB is used for sampling the phase space and exploring possible defect and cluster geometries, one could use sophisticated global optimization algorithms to locate all metastable states and analyse them with more advanced methods to distinguish the true ground state. As COMB itself may give non-physical results, it is not enough to only consider the lowest energy configuration as given by COMB.

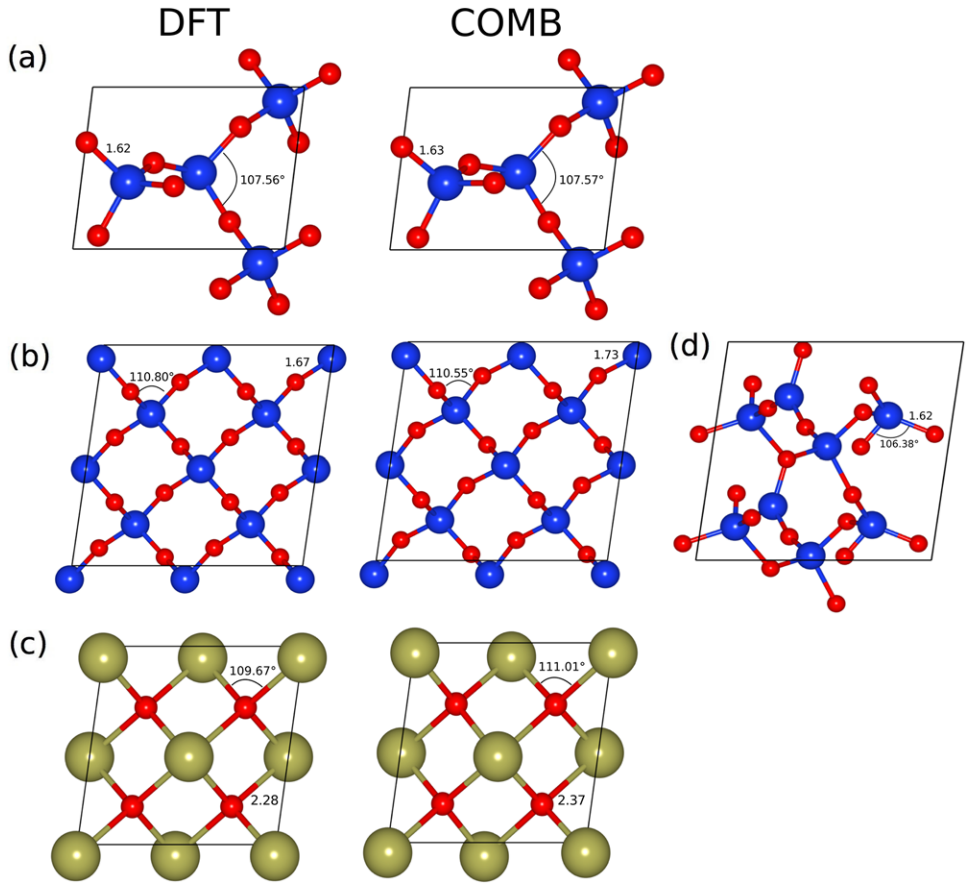

Figure 4. Sheared silica α-quartz (a), β-cristobalite (b), and cubic hafnia (c) lattices according to DFT and COMB. For cristobalite, another metastable structure (d) is also found with COMB.

Since the hierarchy of metastable states may be incorrect in COMB, also the analysis of reaction paths and energy barriers may fail, as it requires a reliable representation of the potential energy surface. This is unfortunate, as mapping the potential energy surface and transition states is a resource intensive task where an atomistic potential could provide substantial gains in computational efficiency. The spurious minima should arguably not be as severe a problem in molecular dynamics simulations, where the system will not be in an energy minimum in any case. Naturally, errors in the potential energy will lead to different molecular trajectories, but overall the system should behave realistically if the COMB structures do not differ too wildly from realistic ones. This means that approaches using, for example, simulated annealing using the COMB approach may provide reasonable starting points for more advanced methods.

To summarize, COMB is found to have substantial shortcomings when describing small clusters and defects, where the local bonding environment is different compared to the bulk. The results obtained with COMB are plausible, but at least against a DFT benchmark they are in many cases incorrect. As a result, we conclude that COMB is likely suitable for calculating bulk properties and possibly also finite temperature simulations such as annealing, but it

lacks predictive power and results obtained with COMB should be further verified with more advanced methods if low coordinated structures are present in the system.

Acknowledgments

The authors acknowledge funding from EU project MORDRED (Grant No. 261868) and the computational resources provided by the Aalto Science-IT project and CSC-IT Center for Science, Finland. TM acknowledges financial support from the Academy of Finland through its Centres of Excellence Programme (2012–2017) under Project No. 251748 and The Finnish Academy of Science and Letters, Vilho, Yrjö and Kalle Väisälä Foundation.

References

[1] Burke K 2012 *J. Chem. Phys.* **136** 150901
[2] Goringe C M, Bowler D R and Hernàndez E 1997 *Rep. Prog. Phys.* **60** 1447
[3] Bush T S, Gale J D, Catlow C R A and Battle P D 1994 *J. Mater. Chem.* **4** 831
[4] Mackerell A D 2004 *J. Comput. Chem.* **25** 1584
[5] Harding J H, Duffy D M, Sushko M L, Rodger P M, Quigley D and Elliott J A 2008 *Chem. Rev.* **108** 4823
[6] Liang T *et al* 2013 *Annu. Rev. Mater. Res.* **43** 109
[7] van Duin A, Dasgupta S, Lorant F and Goddard W 2001 *J. Phys. Chem.* A **105** 9396
[8] Yu J, Sinnott S B and Phillpot S R 2007 *Phys. Rev.* B **75** 085311
[9] Liang T, Devine B, Phillpot S R and Sinnott S B 2012 *J. Phys. Chem.* A **116** 7976
[10] Shan T R, Bryce D, Hawkins J, Asthagiri A, Phillpot S and Sinnott S 2010 *Phys. Rev.* B **82** 235302
[11] Shan T R, Devine B D, Kemper T W, Sinnott S B and Phillpot S R 2010 *Phys. Rev.* B **81** 125328
[12] Devine B, Shan T R, Cheng Y T, McGaughey A, Lee M, Phillpot S and Sinnott S 2011 *Phys. Rev.* B **84** 125308
[13] Cheng Y T, Shan T R, Devine B, Lee D, Liang T, Hinojosa B B, Phillpot S R, Asthagiri A and Sinnott S B 2012 *Surf. Sci.* **606** 1280
[14] Buckingham R A 1938 *Proc. R. Soc.* A **168** 264
[15] Daw M S and Baskes M 1984 *Phys. Rev.* B **29** 6443
[16] Tersoff J 1988 *Phys. Rev.* B **37** 6991
[17] Brenner D W 1990 *Phys. Rev.* B **42** 9458
[18] Behler J and Parrinello M 2007 *Phys. Rev. Lett.* **98** 146401
[19] Bartók A P, Payne M C and Csányi G 2010 *Phys. Rev. Lett.* **104** 136403
[20] International Technology Roadmap for Semiconductors www.itrs2.net accessed: 2015-09-25
[21] Wilk G D, Wallace R M and Anthony J M 2001 *J. Appl. Phys.* **89** 5243–75
[22] Robertson J 2005 *Solid-State Electron.* **49** 283
[23] Ribes G, Mitard J, Denais M, Bruyere S, Monsieur F, Parthasarathy C, Vincent E and Ghibaudo G 2005 *IEEE Trans. Dev. Mater. Reliab.* **5** 5
[24] El-Sayed A M, Watkins M B, Grasser T, Afanas'ev V V and Shluger A L 2015 *Phys. Rev. Lett.* **114** 115503
[25] Gerrer L, Ling S, Amoroso S M, Asenov P, Shluger A L and Asenov A 2013 *J. Comput. Electron.* **12** 638
[26] Nayak S K, Rao B K, Khanna S N and Jena P 1998 *J. Chem. Phys.* **109** 1245
[27] Wang L S, Nicholas J B, Dupuis M, Wu H and Colson S D 1997 *Phys. Rev. Lett.* **78** 4450
[28] Chu T S, Zhang R Q and Cheung H F 2001 *J. Phys. Chem.* B **105** 1705
[29] Foster A S, Gejo F L, Shluger A L and Nieminen R M 2002 *Phys. Rev.* B **65** 174117
[30] McKenna K and Shluger A 2009 *Appl. Phys. Lett.* **95** 222111
[31] Zheng J X, Ceder G, Maxisch T, Chim W K and Choi W K 2007 *Phys. Rev.* B **75** 104112
[32] Rick S W, Stuart S J and Berne B J 1994 *J. Chem. Phys.* **101** 6141
[33] Shan T R, Devine B D, Phillpot S R and Sinnott S B 2011 *Phys. Rev.* B **83** 115327
[34] Roothaan C C J 1951 *J. Chem. Phys.* **19** 1445
[35] Wolf D, Keblinski P, Phillpot S and Eggebrecht J 1999 *J. Chem. Phys.* **110** 8254

[36] Kresse G and Furthmüller J 1996 *Phys. Rev.* B **54** 11169
[37] Blöchl P E 1994 *Phys. Rev.* B **50** 17953
[38] Kresse G and Joubert D 1999 *Phys. Rev.* B **59** 1758
[39] Perdew J P, Burke K and Ernzerhof M 1996 *Phys. Rev. Lett.* **77** 3865
[40] Henkelman G, Arnaldsson A and Jónsson H 2006 *Comput. Mater. Sci.* **36** 354
[41] Tang W, Sanville E and Henkelman G 2009 *J. Phys.: Condens. Matter* **21** 084204
[42] Plimpton S 1995 *J. Comput. Phys.* **117** 1
[43] Hynninen T, Himanen L, Parkkinen V, Musso T, Corander J and Foster A S 2016 *Comput. Phys. Commun.* **198** 230
[44] Neumayer D and Cartier E 2001 *J. Appl. Phys.* **90** 1801
[45] Foster A S, Shluger A L and Nieminen R M 2002 *Phys. Rev. Lett.* **89** 225901
[46] Vos M, Grande P L, Venkatachalam D K, Nandi S K and Elliman R G 2014 *Phys. Rev. Lett.* **112** 175901
[47] Ghasemi S A, Amsler M, Hennig R G, Roy S, Goedecker S, Lenosky T J, Umrigar C J, Genovese L, Morishita T and Nishio K 2010 *Phys. Rev.* B **81** 214107